CEBAF PR-91-012
April 1991

An Autocorrelation Technique for Measuring Sub-Picosecond Bunch Length Using Coherent Transition Radiation

Walter Barry
Continuous Electron Beam Accelerator Facility
12000 Jefferson Avenue
Newport News, VA 23606

CONTINUOUS ELECTRON BEAM ACCELERATOR FACILITY

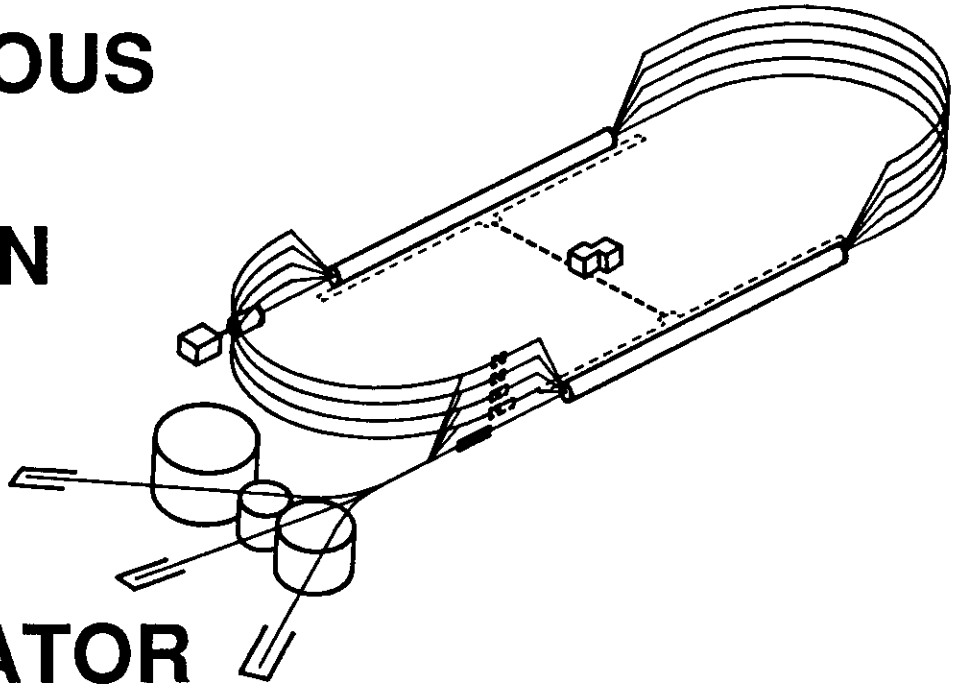

SURA *Southeastern Universities Research Association*

CEBAF
The Continuous Electron Beam Accelerator Facility

Newport News, Virginia

Copies available from:

Library
CEBAF
12000 Jefferson Avenue
Newport News
Virginia 23606

The Southeastern Universities Research Association (SURA) operates the Continuous Electron Beam Accelerator Facility for the United States Department of Energy under contract DE-AC05-84ER40150.

An Autocorrelation Technique for Measuring Sub-Picosecond Bunch Length Using Coherent Transition Radiation*

Walter Barry
Continuous Electron Beam Accelerator Facility
12000 Jefferson Avenue, Newport News, Virginia 23606

Abstract

A new technique for determining sub-picosecond bunch length using infrared transition radiation and interferometry is proposed. The technique makes use of an infrared Michelson interferometer for measuring the autocorrelation of transition radiation emitted from a thin conducting foil placed in the beam path. The theory of coherent radiation from a charged particle beam passing through a thin conducting foil is presented. Subsequently, the analysis of this radiation through Michelson interferometry is shown to provide the autocorrelation of the longitudinal bunch profile. An example relevant to the CEBAF front end test is discussed.

Introduction

It is well known that transition radiation is a phenomenon useful for measuring various parameters of a charged particle beam including energy, emittance and transverse profile.[1] Typically, these measurements are made in the optical region where the radiation is due to individual charged particle effects.

In order to determine the collective longitudinal properties of a particle beam, i.e., bunch length and longitudinal profile, a device or system capable of measuring the temporal or longitudinal spatial distribution of the bunch charge or current is required. One common method of measuring longitudinal profile makes use of optical radiation (synchrotron, transition or Cherenkov) and a streak camera. This "single shot" technique is quite expensive and generally limited to 1-2 psec bunch lengths. Alternatively, by considering radiation in the region where wavelength is comparable to bunch length and bunch to bunch coherence is exhibited (wavelengths large compared to particle spacing), autocorrelation or spectral analysis techniques can be used to measure equivalent bunch widths. For picosecond and shorter bunches, this region generally covers the infrared.

In this note, a technique for measuring the autocorrelation of longitudinal bunch profile using infrared transition radiation from a conducting foil and Michelson interferometry is described. In order to present a clear picture of the origin and properties of transition radiation, the radiation from an arbitrary charge distribution striking a conducting foil is derived in some detail. Subsequently, the analysis of this radiation through Michelson interferometry is shown to provide the autocorrelation of the longitudinal bunch profile. An example relevant to the measurement of bunch length at CEBAF is given.

* Work supported by U.S. Department of Energy under contract DE-AC05-84ER40150.

Radiation from a Conducting Foil

Consider a beam of charged particles with velocity βc in the $\hat{z}$ direction striking a conducting foil located at the $z = 0$ plane in the cylindrical coordinate system (figure 1). The foil is assumed to be perfectly conducting and the beam filamentary along the z axis. For radiation wavelengths large compared to particle spacing, the beam is well approximated by a moving line charge distribution $q_\ell(t - z/\beta c)$, where $q_\ell(t)$ is the charge distribution of the beam measured as a function of time as the beam passes the $z = 0$ plane. Accordingly, the beam current is defined as $I_0(t - z/\beta c) = \beta c q_\ell(t - z/\beta c)$. For the autocorrelation measurement described later, the charge distribution must be periodic. However, this restriction is not necessary for the radiation derivation.

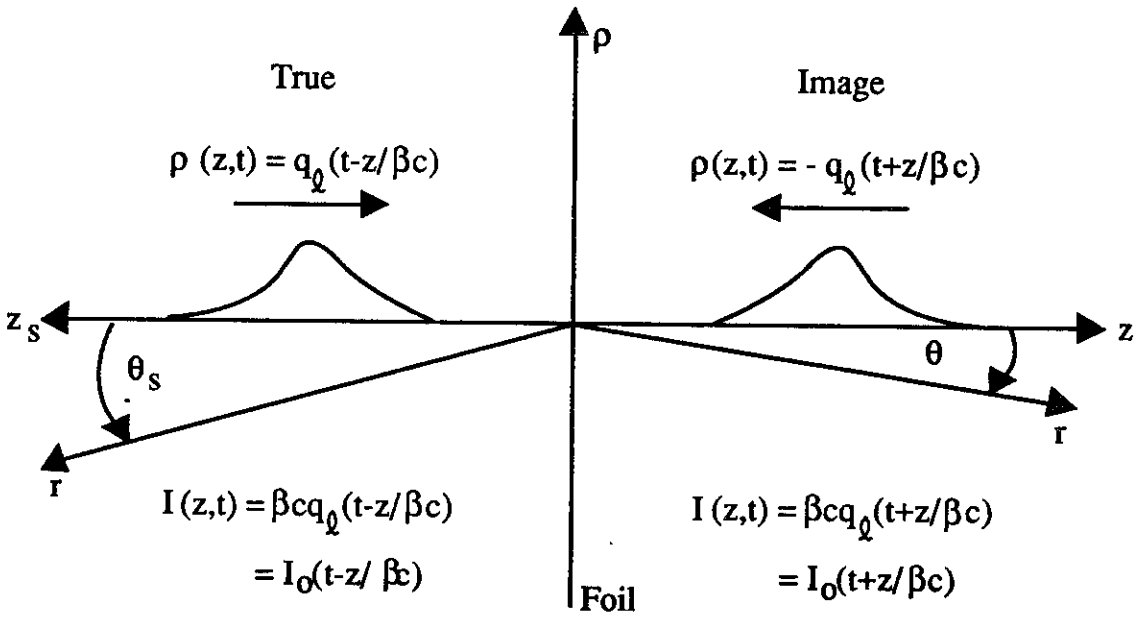

Figure 1. Image method for radiation from a thin foil.

In order to satisfy boundary conditions at the conducting plane, surface currents are induced in response to the fields of the incident beam. These currents in turn radiate electromagnetic energy. Thus, in general, transition radiation can be described as a reaction to boundary conditions. Traditionally, the term transition radiation refers to radiation emitted from a charged particle as it passes from one medium to another (in this case vacuum to metal). However, radiation of this type will occur when any current distribution is in the presence of abrupt boundary conditions. Unusual examples of transition radiation might include radiation from a beam passing through a conducting aperture or from a slot in the wall of a uniform beam chamber. The spatial and frequency characteristics of the radiation are, of course, extremely dependent on the boundary geometry.

As indicated in figure 1, a convenient technique for solving the foil radiation problem makes use of image theory. Here, the conducting foil is removed and an image current

$I_0(t + z/\beta c)$ is inserted for $z \geq 0$ so that:

$$I(z,t) = \begin{cases} I_0(t + z/\beta c) & z \geq 0 \\ I_0(t - z/\beta c) & z \leq 0 \end{cases} \tag{1}$$

With this current, it is clear that only the z component of vector potential exists and from symmetry, the vector potential and the fields derived from it are independent of ϕ.

The vector potential must satisfy the homogeneous wave equation for $\rho > 0$:

$$\nabla^2 A_z(\rho,z,t) - \frac{1}{c^2}\frac{\partial^2 A_z(\rho,z,t)}{\partial t^2} = 0 \quad \rho > 0 \tag{2}$$

subject to the excitation condition:

$$\lim_{\rho \to 0} \int_0^{2\pi} H_\phi(\rho,z,t)\rho \, d\phi = I(z,t) \tag{3}$$

The procedure for solving (2) is greatly simplified by introducing the two dimensional Fourier transform:

$$\tilde{f}(\rho,\eta,\omega) = \int_{-\infty}^{\infty} \int_{-\infty}^{\infty} f(\rho,z,t)e^{-j(\omega t+\eta z)} \, dt \, dz \tag{4}$$

which has an inversion given by:

$$f(\rho,z,t) = \frac{1}{4\pi^2} \int_{-\infty}^{\infty} \int_{-\infty}^{\infty} \tilde{f}\,(\rho,\eta,\omega)\, e^{j(\omega t+\eta z)} \, d\omega d\eta \tag{5}$$

Applying (4) to (1), (2) and (3) results in a statement of the problem in the transform domain:

$$\frac{\partial^2 \tilde{A}_z\,(\rho,\eta,\omega)}{\partial \rho^2} + \frac{1}{\rho} \frac{\partial \tilde{A}_z(\rho,\eta,\omega)}{\partial \rho} + (k_0^2 - \eta^2)\tilde{A}_z(\rho,\eta,\omega) = 0 \tag{6}$$

$$\lim_{\rho \to 0} \int_0^{2\pi} \tilde{H}_\phi(\rho,\eta,\omega)\, \rho d\phi = \frac{-j2k\bar{I}_0(\omega)}{\eta^2 - k^2} \tag{7}$$

$$\text{where : } k = k_0/\beta = \omega/\beta c$$

$\bar{I}_0(\omega)$ is the frequency spectrum of the current defined by:

$$\bar{I}_0(\omega) = \int_{-\infty}^{\infty} I_0(t)e^{-j\omega t} \, dt \tag{8}$$

with inversion:

$$I_0(t) = \frac{1}{2\pi} \int_{-\infty}^{\infty} \bar{I}_0(\omega)e^{j\omega t} \, d\omega \tag{9}$$

Equation (6) is Bessel's equation of order zero. Anticipating outward propagating wave characteristics, a solution to (6) is:

$$\tilde{A}_z(\rho,\eta,\omega) = c(\eta,\omega)H_0^{(2)}\left(\rho\sqrt{k_0^2-\eta^2}\right) \tag{10}$$

where: $H_0^{(2)}(x)$ = zero order Hankel function of the second kind

$c(\eta,\omega)$ = function to be determined by excitation condition

The ϕ component of the $\vec{H}$ field can be derived from the vector potential using:

$$\tilde{H}_\phi(\rho,\eta,\omega) = -\frac{1}{\mu_0}\ \frac{\partial\tilde{A}_z(\rho,\eta,\omega)}{\partial\rho} \tag{11}$$

Using equations (10), (11) and (7) and the small argument approximation for $H_1^{(2)}(x)$ yields the following expression for $c(\eta,\omega)$:

$$c(\eta,\omega) = \frac{-\mu_0\bar{I}_0(\omega)}{2}\ \left(\frac{k}{\eta^2-k^2}\right) \tag{12}$$

Therefore, from (10):

$$\tilde{A}_z(\rho,\eta,\omega) = \frac{-\mu_0\bar{I}_0(\omega)}{2}\ \left(\frac{k}{\eta^2-k^2}\right)\ H_0^{(2)}\left(\rho\sqrt{k_0^2-\eta^2}\right) \tag{13}$$

Taking the $\eta \rightarrow z$ part of the inversion given in (5) yields:

$$\bar{A}_z(\rho,z,\omega) = \frac{-\mu_0\bar{I}_0(\omega)}{4\pi}\ \int_{-\infty}^{\infty}\left(\frac{k}{\eta^2-k^2}\right)\ H_0^{(2)}\left(\rho\sqrt{k_0^2-\eta^2}\right)e^{j\eta z}\,d\eta \tag{14}$$

Equation (14) gives, in integral form, the exact frequency domain expression for the vector potential. For the purpose of evaluating the fields in the radiation zone (ρ and z large), the integral in (14) may be approximated by the method of stationary phase (appendix I) giving:

$$\bar{A}_z(r,\theta,\omega) = \frac{-j\mu_0\bar{I}_0(\omega)e^{-jk_0r}}{2\pi r}\ \left(\frac{k}{k_0^2\cos^2\theta-k^2}\right) \qquad k_0r \gg 1 \tag{15}$$

where: $z = r\cos\theta$

$\rho = r\sin\theta$

As indicated in figure 1, r and θ are spherical coordinates with θ measured from the $+z$ axis. As is usual with the method of images, the actual fields are those obtained for the region containing the true charge or $z \leq 0$. Accordingly, it is convenient to use the axis of specular reflection ($z_s = -z$) as a reference when expressing the vector potential and fields. Equation (15) is then written:

$$\bar{A}_{z_s}(r,\theta_s,\omega) = \frac{j\mu_0 \bar{I}_0(\omega) e^{-jk_0 r}}{2\pi r} \left(\frac{k}{k_0^2 \cos^2\theta_s - k^2} \right) \qquad k_0 r \gg 1 \tag{16}$$

where θ_s and z_s are as shown in figure 1. The electric and magnetic fields may be obtained in the typical manner using:

$$\vec{H}(r,\theta_s,\omega) = \frac{1}{\mu_0} \nabla \times \vec{A}(r,\theta_s,\omega) \tag{17}$$

$$\vec{E}(r,\theta_s,\omega) = -j\omega \vec{A}(r,\theta_s,\omega) + \frac{\nabla\nabla \cdot \vec{A}(r,\theta_s,\omega)}{j\omega\mu_0\epsilon_0} \tag{18}$$

Resolving (16) into $\hat{r}$ and $\hat{\theta}_s$ components, substituting into (17) and (18) and retaining only $1/r$ terms, expressions for the radiation fields are found:

$$\bar{E}_{\theta_s}(r,\theta_s,\omega) = \frac{Z_0 \bar{I}_0(\omega) e^{-jk_0 r}}{2\pi r} \left(\frac{\beta \sin\theta_s}{1 - \beta^2 \cos^2\theta_s} \right) \tag{19}$$

$$\bar{H}_{\phi_s}(r,\theta_s,\omega) = \frac{\bar{E}_{\theta_s}(r,\theta_s,\omega)}{Z_0} \tag{20}$$

$$\text{where :} \quad Z_0 = \sqrt{\frac{\mu_0}{\epsilon_0}} = 377\Omega$$

Equations (19) and (20) are the frequency domain field expressions for backward transition radiation emitted from a beam striking a conducting foil. It should be pointed out that in the previous analysis, the thickness of the foil is irrelevant. If, however, the foil is thin so that the beam passes through unperturbed, radiation will also be emitted in the forward direction. The forward fields are obtained by reversing the ranges of z in (1). The results are identical to (19) and (20) with the simple substitutions $\theta_s \rightarrow \theta$ and $\phi_s \rightarrow \phi$. The autocorrelation technique described in the next section requires only backward radiation, therefore, forward radiation from thin foils will not be pursued.

Several important features of transition radiation are evident from equations (19) and (20). From (19) it is seen that the frequency spectrum of the radiation is identical to that of the beam current. Therefore, the conducting foil can be viewed as a device that produces a propagating electromagnetic wave that is an exact replica in time of the incident beam current (an infinite bandwidth antenna). This feature is most easily seen by transforming (19) and (20) to the time domain via (9):

$$E_{\theta_s}(r,\theta_s,t) = \frac{Z_0 I_0(t - r/c)}{2\pi r} \left(\frac{\beta \sin\theta_s}{1 - \beta^2 \cos^2\theta_s} \right) \tag{21}$$

$$H_{\phi_s}(r,\theta_s,t) = \frac{E_{\theta_s}(r,\theta_s,t)}{Z_0} \tag{22}$$

Comparing the above equations to (1) shows that at a fixed point r in space, the radiation has the same temporal characteristics as the beam current for a fixed point z. It is this property that makes the autocorrelation measurement, to be described, possible.

Another important characteristic of transition radiation is its spatial distribution. From (21), it is clear that the angular distribution of energy or power density is given by the function:

$$S^2(\theta_s) = \left(\frac{\beta \sin\theta_s}{1-\beta^2\cos^2\theta_s}\right)^2 \tag{23}$$

This function has a single, very sharp maximum at $\theta_s = 1/\beta\gamma$. Therefore, for relativistic beams, virtually all of the radiation is in the vicinity of this extremely small angle. In this case, an excellent approximation for $S^2(\theta_s)$ is:

$$S^2(\theta_s) \approx \left(\frac{\theta_s}{1/\gamma^2+\theta_s^2}\right)^2 \qquad \gamma \text{ large} \tag{24}$$

From (24) it is noted that the energy or power density is proportional to γ^2 at $\theta_s \approx 1/\gamma$.

The standard example of transition radiation is that of a single electron striking the foil. In this case, the current is approximated by $I_0(t) = e\delta(t)$ so that $I_0(\omega) = e$. For a single electron or pulse of current, it is convenient to calculate the radiated energy per unit frequency per unit solid angle:

$$\frac{\partial^2 U}{\partial\omega\partial\Omega} = \frac{|\tilde{E}_{\theta_s}(r,\theta_s,\omega)|^2}{2\pi Z_0}\, r^2 \tag{25}$$

Substituting (19) with $I_0(\omega) = e$ into (25) yields the standard formula for transition radiation from a single electron striking a foil:

$$\frac{\partial^2 U_e}{\partial\omega\partial\Omega} = \frac{e^2 Z_0}{8\pi^3}\, S^2(\theta_s) \qquad \frac{\text{Joule}}{\text{Hz}\cdot\text{Steradian}} \tag{26}$$

From (26) it is seen that for this idealized calculation, the electron radiates uniformly over the entire spectrum. In reality, the analysis presented breaks down at wavelengths comparable to the microstructure of the foil. However, for highly polished foils, (26) is taken to be a reasonable approximation for wavelengths well into the visible range.

Because electrons in an accelerator are randomly distributed from bunch to bunch, autocorrelation of optical transition radiation will not provide any information on bunch length or profile. However, autocorrelation of transition radiation at wavelengths comparable to bunch length will provide this information if the bunch length is large compared to electron spacing. This latter requirement ensures bunch to bunch coherence of the radiation. In this case $I_0(t)$ is a simple periodic current corresponding to a continuous train of bunches passing through the foil.

By use of equations (21) and (22) and the definition of the Poynting vector, the total average power per unit solid angle radiated by a periodic beam current, $I_0(t)$, striking a foil can be found:

$$\frac{dP}{d\Omega} = \frac{P_{Z_0}}{4\pi^2} S^2(\theta_*) \qquad \text{watts/steradian} \tag{27}$$

where:

$$P_{Z_0} = \frac{Z_0}{T} \int_T I_0^2(t)dt \qquad T = \text{period of } I_0(t) \tag{28}$$

The quantity P_{Z_0} is recognized as the total average power dissipated by $I_0(t)$ in a 377Ω (free space) resistor. By integrating (27) over the backward radiation half space, the total radiated power for a relativistic beam is obtained:

$$P \approx \frac{P_{Z_0} ln\gamma}{2\pi} \qquad \text{watts} \tag{29}$$

The frequency spectrum of P consists of discrete lines at integer multiples of $1/T$ with amplitudes proportional to the square of the Fourier transform of the bunch profile. In this case, it is clear that the critical frequency components for determining bunch profile and length are in the $1/\tau_b$ region. This region covers the far infrared for the approximate range of bunch lengths, .03 psec $\leq \tau_b \leq$ 3 psec. It is worthwhile to note that power measurements in the far infrared are traditionally made with bolometric and other heat measuring devices. Because heat is measured, these devices are "flat" in the power measurement sense throughout the far infrared range. Therefore, through interferometry or filtering, the autocorrelation or power spectrum of bunch profile may be obtained using these devices as detectors. The lower limits on sensitivity for these devices range from 10^{-8} watts for the simplest thermocouple devices to 10^{-11} watts for cryogenic detectors.[2]

As an example relevant to CEBAF, consider a beam current consisting of a continuous train of bunches with uniform rectangular profiles of length τ_b. The period of $I_0(t)$ (time between bunches) is T and the average current is I_{av}. In this case, it is easy to show that:

$$P_{Z_0} = \frac{Z_0 I_{av}^2 T}{\tau_b} \quad \text{watts} \tag{30}$$

A typical front end test beam might have the parameters $I_{av} = 100 \times 10^{-6}$ amps, $T/\tau_b =$ 360 and $\gamma = 88$ (45 MeV). With these parameters and equations (29) and (30), the total power radiated from the foil is 1mW. This level is certainly detectable by any of the devices mentioned above. In addition, from equation (27), the angular distribution of power, shown in figure 2, can be plotted. As expected, the radiation is concentrated in a thin cone of half angle $1/\gamma = 11$ mrad with a peak angular power density of 67 mW/steradian. As will be seen, the high directionality of the radiation is important for the autocorrelation measurement described in the next section.

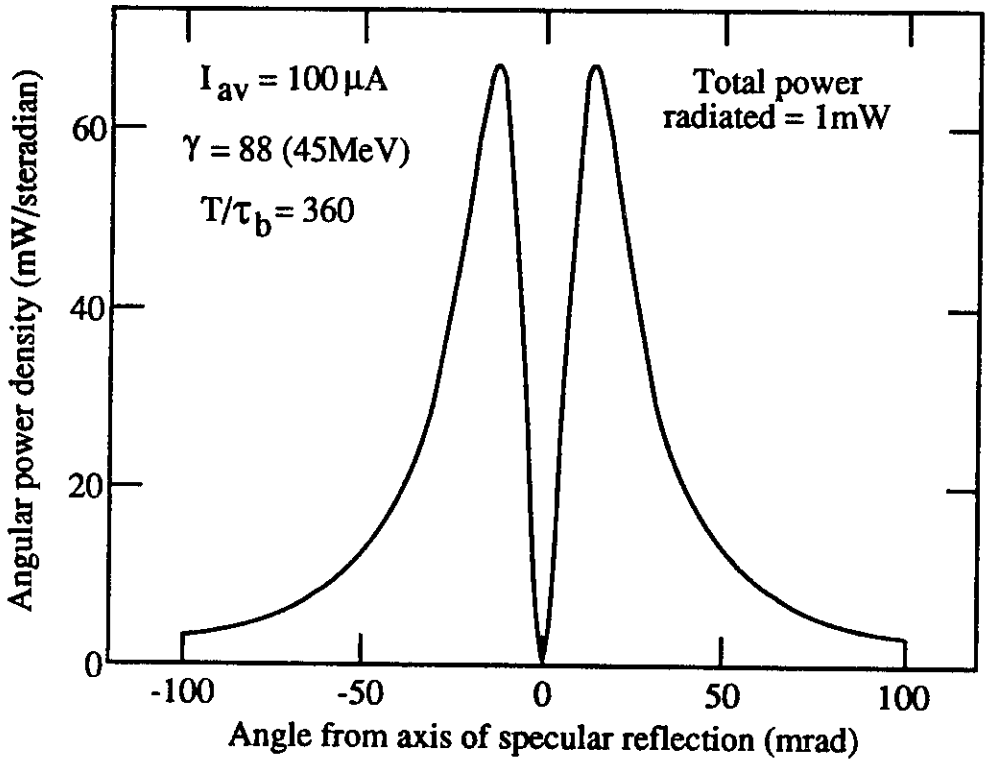

Figure 2. Thin foil radiation from a typical CEBAF front end test beam.

Autocorrelation of Bunch Profile Through Michelson Interferometry

A simple system for obtaining the autocorrelation of the beam current is shown in figure 3. Here, the beam current, $I_0(t)$, passes through a thin conducting foil at an incident angle of 45°. Backward transition radiation is then emitted about the axis of specular reflection and directed into an infrared Michelson interferometer. By measuring power at the output port of the interferometer as a function of Δ in the delay path, the autocorrelation of $I_0(t)$ may be obtained. It is important to note that in general, the transition radiation field expressions for oblique incidence are considerably more complicated than those for normal incidence. However, as shown in Appendix II, for large γ, the field expressions about the axis of specular reflection are well approximated by the normal incidence expressions derived in the previous section.

The interferometer, illustrated in figure 3, consists of a fixed mirror, a movable mirror and a splitter/combiner. These elements are arranged so that the incoming radiation is split into two beams. One of the beams is then delayed by a distance Δ before recombination takes place at the output port. In order to simplify the analysis of the interferometer, the optical elements are assumed to be non-dispersive. If the mirrors and splitter/combiner are modeled as thin conductive surfaces, it can be shown that the reflection and transmission coefficients for these elements are the same for incident waves with polarization in the plane of incidence and normal to the plane of incidence except for an overall sign change with the reflection coefficient. Because power is being measured, the sign difference between the

reflection coefficients for the two polarizations is irrelevant. Therefore, the optical elements can be characterized by single reflection and transmission coefficients which are valid for all incident polarizations. As indicated in figure 3, the transmission coefficients for the splitter/combiner are designated as S_{11} and S_{21}, respectively. Both mirrors have reflection coefficients of 1.

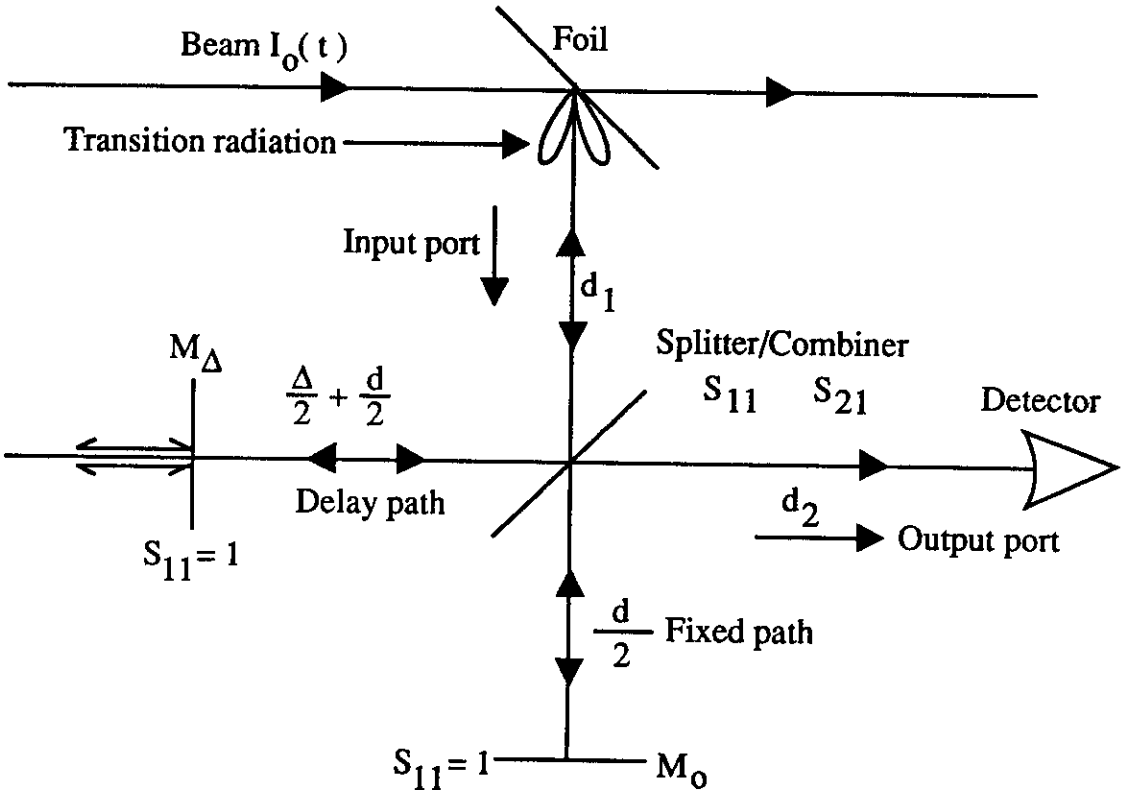

Figure 3. Michelson interferometer.

The simplest way to determine the power measured by the detector is to image the radiation source at the foil into two sources separated by a distance Δ (figure 4). As shown in figure 4, image source 1 corresponds to the fixed path in the interferometer while image source 2 corresponds to the variable delay path. In this case, the fields at a point p_0 at the detector due to each source are given by:

$$\vec{E}_1(r_1, \theta_1, \omega) = \frac{S_{11} S_{21} Z_0 \bar{I}_0(\omega)}{2\pi r_1} e^{-jk_0 r_1} S(\theta_1) \hat{\theta}_1 \tag{31}$$

$$\vec{E}_2(r_2, \theta_2, \omega) = \frac{S_{11} S_{21} Z_0 \bar{I}_0(\omega)}{2\pi r_2} e^{-jk_0 r_2} S(\theta_2) \hat{\theta}_2 \tag{32}$$

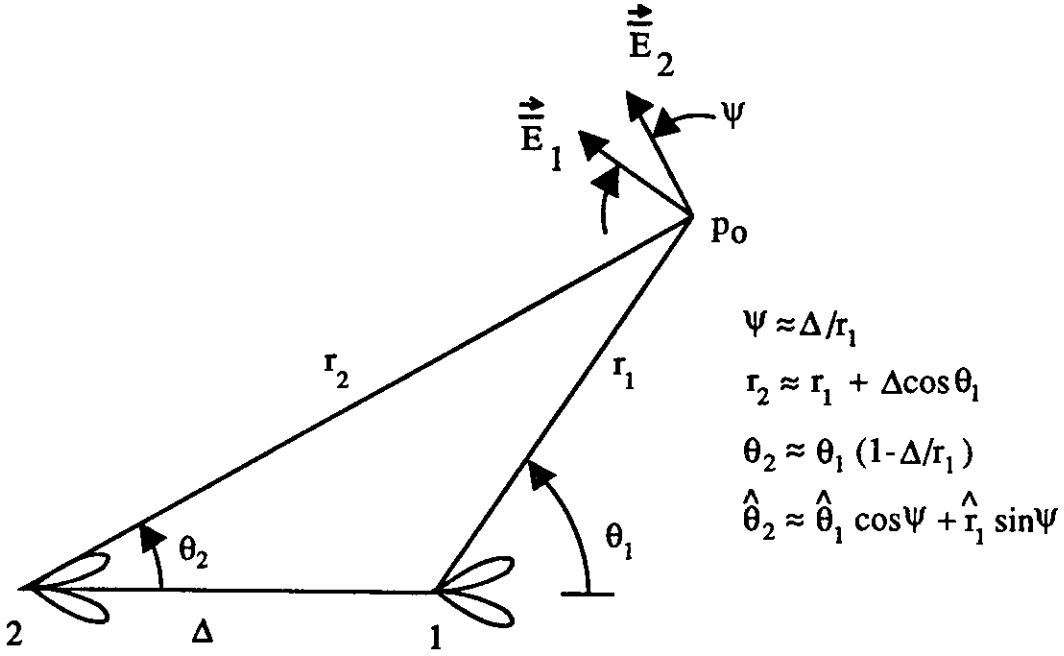

Figure 4. Source imaged through interferometer.

The pertinent coordinate and unit vector transformations between systems 1 and 2 are indicated in figure 4. These relations were derived using small angle approximations and $\Delta << r_1, r_2$. In fact, θ_1 and θ_2 are both on the order of $1/\gamma$ which is extremely small. In addition, Δ, which is on the order of the bunch length is extremely small compared to r_1 and r_2 which are both approximately equal to the total distance from the foil to the detector including all reflections in the interferometer. Therefore, the transformations given in figure 4 may be further approximated as follows: $r_2 = r_1 \equiv r$ for magnitudes, $r_2 = r_1 + \Delta \equiv r + \Delta$ for phases, $\theta_2 = \theta_1 \equiv \theta$ and $\hat{\theta}_2 = \hat{\theta}_1 \equiv \hat{\theta}$. Using these approximations, the total electric field at p_0 becomes:

$$\vec{E}\ (r,\theta,\omega) = \vec{E}_1 + \vec{E}_2 = \frac{S_{11}S_{21}Z_0\bar{I}_0(\omega)}{2\pi r}e^{-jk_0r}(1+e^{-jk_0\Delta})S(\theta)\hat{\theta} \tag{33}$$

Dropping the overall phase factors in (33) and transforming to the time domain yields:

$$E_\theta(r,\theta,t) = \frac{|S_{11}S_{21}|Z_0S(\theta)}{2\pi r}\Big[I_0(t) + I_0(t-\tau)\Big] \tag{34}$$

where $\tau = \Delta/c$. Because the radiation is confined to a cone of half angle $1/\gamma$, it may be assumed that the detector measures the total available power. In this case, the total power detected as a function of τ becomes:

$$P_d(\tau) = \frac{|S_{11}S_{21}|^2 ln\gamma}{\pi}\Big[P_{Z_0} + \frac{Z_0}{T}\int_T I_0(t)I_0(t-\tau)dt\Big] \tag{35}$$

where P_{Z_0} is defined in (28).

Clearly, the second term in the brackets of equation (35) represents the autocorrelation of the beam current, which in turn is proportional to the autocorrelation of the bunch profile repeated periodically with period T. As an example, $P_d(\tau)$ for the CEBAF beam described in the previous section is plotted in figure 5. In figure 5, the typical value of $|S_{11}S_{21}|^2 = .09$ for a half silvered splitter/combiner has been used. As shown, the autocorrelation of a uniform rectangular bunch is the well known triangle function. In this case, the base width of the autocorrelation is twice the width of the rectangular bunch. Typically, $\tau_b = 1.8$ psec for the CEBAF beam.

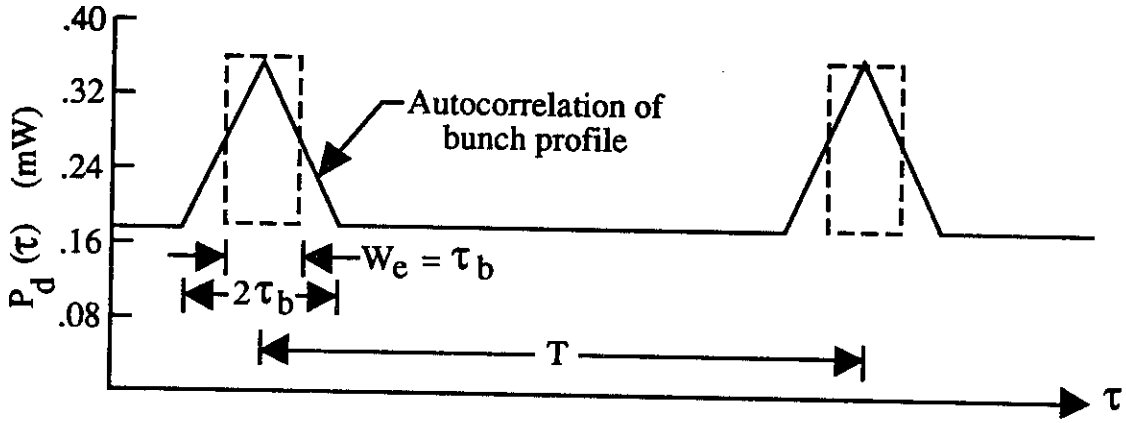

Figure 5. Output from interferometer for CEBAF front end test beam.

Ascertaining information about a function, $f(t)$, from its autocorrelation, $F(\tau)$, is a common problem in many branches of physics and engineering. Because the autocorrelation is obtained by a power measurement, all phase information is lost making it impossible to construct $f(t)$ from $F(\tau)$. However, because $F(\tau)$ is essentially a smoothed out version of $f(t)$, a significant amount of qualitative information about $f(t)$ is obtainable from the autocorrelation.

In addition to providing a qualitative feel for bunch profile, the autocorrelation function can be used to obtain a quantitative measure of bunch length. There are a multitude of quantitative definitions for the width of a function in common usage.[3] One definition which is particularly suitable for describing bunch length is equivalent width, defined as:

$$W_e = \frac{\int_{-\infty}^{\infty} g(x)dx}{g(x_{max})} \tag{36}$$

From (36) it is seen that W_e is the width of a rectangle of height equal to the maximum value of $g(x)$ and of area equal to the area under $g(x)$. As indicated in figure 5, the equivalent width for a uniform rectangular bunch profile is invariant under autocorrelation. Therefore, since most bunch profiles are expected to be close to rectangular, the equivalent width of the autocorrelation is an excellent measure of bunch length. When considering

bunches whose profiles are significantly different from rectangular, the definition of bunch length becomes somewhat arbitrary. Therefore, in all cases, it is not entirely unreasonable to define bunch length as the equivalent width of the autocorrelation. Finally, it is mentioned that the bunch spectrum is easily obtained by taking the Fourier transform of the autocorrelation.

Present and Future Efforts

Efforts are presently being directed towards experimentally verifying the theory presented here by performing a series of experiments at the 45MeV point of the CEBAF front end test. By replacing one of the standard phosphorescent view screens with a thin conducting foil, the emission of transition radiation in both the infrared and visible regions will be verified. Concurrently, an investigation into the design or purchase of a suitable interferometer will be conducted so that ultimately, a bunch length measurement can be made using this technique.

Acknowledgements

The author wishes to express his gratitude to Peter Kloeppel and Geoffrey Krafft of CEBAF for many useful and always interesting discussions.

References

[1] L. Wartski, S. Roland, J. Lasalle, M. Bolore and G. Filippi, "Interference Phenomenon in Optical Transition Radiation and its Application to Particle Beam Diagnostics and Multiple-Scattering Measurements," JAP, vol. 46, pp. 3644-3653, Aug. 1976.

[2] R. A. Smith, F. E. Jones and R. P. Chasmar, "The Detection and Measurement of Infra-Red Radiation," Oxford University Press, Amen House, London, 1960.

[3] R. N. Bracewell, "The Fourier Transform and Its Applications," McGraw-Hill, New York, 1986.

Appendix I

The integral in equation (14) is a specific case of the general form:

$$\psi = \int_{-\infty}^{\infty} g(\eta) H_0^{(2)}(\rho\sqrt{k_0^2 - \eta^2}) e^{j\eta z} d\eta \tag{A.1.1}$$

Using the asymptotic large argument approximation for $H_0^{(2)}(x)$ and transforming to spherical coordinates gives:

$$\psi \approx \sqrt{\frac{2}{\pi r \sin\theta}} e^{j\frac{\pi}{4}} \int_{-\infty}^{\infty} \frac{g(\eta)}{(k_0^2 - \eta^2)^{\frac{1}{4}}} e^{-jr(\sin\theta\sqrt{k_0^2-\eta^2} - \eta\cos\theta)} d\eta \tag{A.1.2}$$

$$\text{where:} \quad z = r\cos\theta$$
$$\rho = r\sin\theta$$

The integral in (A.1.2) has the form of a continuous weighted superposition of radial waves. Examination of the argument of the exponential reveals that propagating waves exist only for $-k_0 \leq \eta \leq k_0$. Outside of this range, the waves decrease or increase exponentially with r. At large r, the exponentially decreasing waves contribute negligibly to the integral and the exponentially increasing waves violate the boundary condition requiring the fields to approach zero as $r \to \infty$. Therefore, (A.1.2.) may be written:

$$\psi \approx \sqrt{\frac{2}{\pi r \sin\theta}} e^{j\frac{\pi}{4}} \int_{-k_0}^{k_0} \frac{g(\eta)}{(k_0^2 - \eta^2)^{\frac{1}{4}}} e^{-jrh(\eta)} d\eta \tag{A.1.3}$$

$$\text{where :} \quad h(\eta) = \sin\theta\sqrt{k_0^2 - \eta^2} - \eta\cos\theta$$

For large r, the exponential term in (A.1.3) oscillates rapidly as a function of η except in regions where $h(\eta)$ exhibits an extremum. Because the multiplying function $g(\eta)(k_0^2 - \eta^2)^{-\frac{1}{4}}$ is comparatively slowly varying, the integral averages roughly to zero except in the neighborhood of these extremum or "stationary phase" points. The stationary phase point(s), η_0, is easily obtained from $h'(\eta_0) = 0$. The result is:

$$\eta_0 = \pm k_0 \cos\theta \tag{A.1.4}$$

Of these two points, $\eta_0 = -k_0\cos\theta$ is used because it corresponds to exclusively outward propagation when substituted into $h(\eta)$.

Because the contributions to the integral in (A.1.3) are basically zero except at η_0, it may be approximated by moving the slowly varying function of η outside the integral and evaluating it at η_0. In addition, $h(\eta)$ may be expanded in a Taylor series about η_0. Retaining only terms up to second order, ψ is now approximated by:

$$\psi \approx e^{j\frac{\pi}{4}} \left(\frac{2}{\pi r \sin\theta}\right)^{\frac{1}{2}} \frac{g(\eta_0)}{(k_0^2 - \eta_0^2)^{\frac{1}{4}}} e^{-jrh(\eta_0)} \int_{-k_0}^{k_0} e^{-j\frac{r}{2}h''(\eta_0)(\eta-\eta_0)^2} d\eta \tag{A.1.5}$$

The remaining integral in (A.1.5) is a Fresnel integral with solution:

$$\int_{-k_0}^{k_0} e^{-j\frac{r}{2}h''(\eta_0)(\eta-\eta_0)^2}d\eta \approx \left(\frac{2\pi}{jrh''(\eta_0)}\right)^{\frac{1}{2}} \quad \text{large } r \tag{A.1.6}$$

Substituting (A.1.6) into (A.1.5) and evaluating $h(\eta_0)$ and $h''(\eta_0)$, the final result is obtained:

$$\psi = \int_{-\infty}^{\infty} g(\eta)H_0^{(2)}(\rho\sqrt{k_0^2-\eta^2})e^{j\eta z}dz \xrightarrow[r\to\infty]{} \frac{j2g(-k_0\cos\theta)}{r}e^{-jk_0r} \tag{A.1.7}$$

From equation (14):

$$g(\eta) = \frac{k}{\eta^2-k^2}$$

Therefore:

$$\bar{A}_z(r,\theta,\omega) = \frac{-j\mu_0\bar{I}_0(\omega)}{2\pi r}e^{-jk_0r}\left(\frac{k}{k_0^2\cos^2\theta-k^2}\right) \tag{A.1.8}$$

Appendix II

In this appendix, the properties of transition radiation for the case of oblique incidence are examined.

Referring to figure A.2-1, consider a line charge distribution, $\rho_1(z_1,t) = q_\ell(t + z_1/\beta c)$, travelling along the z_1 axis at an angle θ_i from the normal to the foil. Corresponding to ρ_1, there will be an image charge distribution, $\rho_2(z_2,t) = -q_\ell(t + z_2/\beta c)$, travelling toward the foil along the z_2 axis. Following the conventions in the main text, the corresponding currents are:

$$I_1(z_1,t) = -\beta c q_\ell(t + z_1/\beta c) = -I_0(t + z_1/\beta c) \tag{A.2.1}$$

$$I_2(z_2,t) = \beta c q_\ell(t + z_2/\beta c) = I_0(t + z_2/\beta c) \tag{A.2.2}$$

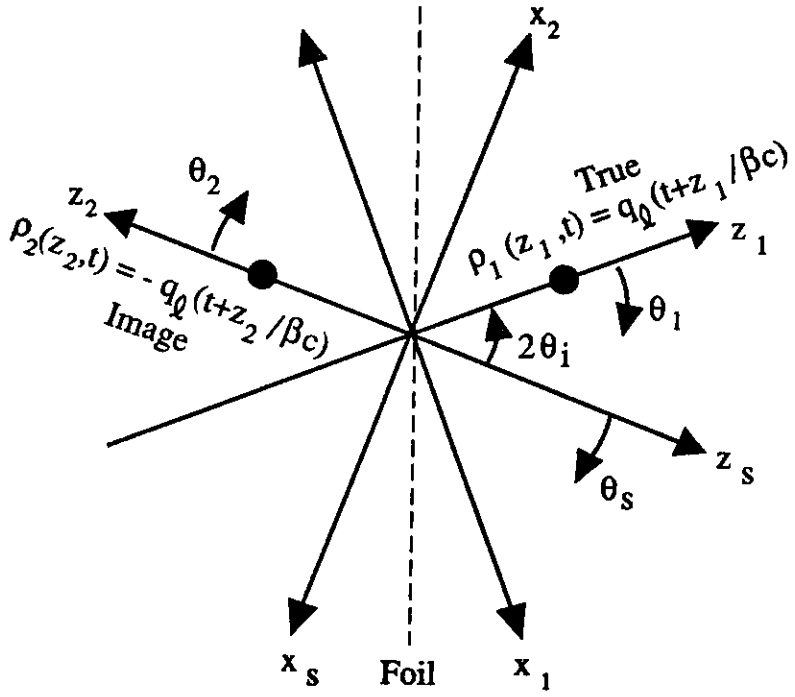

Figure A.2-1. Image geometry for oblique incidence.

Repeating the analysis in the main text for each current individually yields the following vector potentials:

$$\vec{\bar{A}}_1(r_1,\theta_1,\omega) = \frac{-j\mu_0 \bar{I}_0(\omega) e^{-jk_0 r_1}}{4\pi r_1}\left(\frac{1}{k + k_0\cos\theta_1}\right)\hat{z}_1 \tag{A.2.3}$$

$$\vec{\bar{A}}_2(r_2,\theta_2,\omega) = \frac{j\mu_0 \bar{I}_0(\omega) e^{-jk_0 r_2}}{4\pi r_2}\left(\frac{1}{k + k_0\cos\theta_2}\right)\hat{z}_2 \tag{A.2.4}$$

The total vector potential is the sum of (A.2.3) and (A.2.4).

The vector potential may be referred to the axis of specular reflection, z_s, and its associated coordinate system by making the following coordinate and unit vector transformations:

$$\left(\begin{array}{l} r_1 = r_2 = r_s = r \\ \cos\theta_2 = -\cos\theta_s \\ \cos\theta_1 = \cos\theta_s \cos 2\theta_i - \sin\theta_s \cos\phi_s \sin 2\theta_i \\ \hat{z}_2 = -\hat{z}_s \\ \hat{z}_1 = \hat{z}_s \cos 2\theta_i - \hat{x}_s \sin 2\theta_i \end{array}\right) \tag{A.2.5}$$

Substituting these transformations into (A.2.3) and (A.2.4) results in a total vector potential possessing $\hat{x}_s$ and $\hat{z}_s$ components given as follows:

$$\bar{A}_{x_s}(r,\theta_s,\phi_s,\omega) = \frac{j\mu_0 \bar{I}_0(\omega)}{4\pi r}\left[\frac{\sin 2\theta i}{k + k_0(\cos\theta_s \cos 2\theta_i - \sin\theta_s \cos\phi_s \sin 2\theta_i)}\right] e^{-jk_o r} \tag{A.2.6}$$

$$\bar{A}_{z_s}(r,\theta_s,\phi_s,\omega) = \frac{-j\mu_0 \bar{I}_0(\omega)}{4\pi r}\left[\frac{1}{k - k_0\cos\theta_s} + \frac{\cos 2\theta i}{k + k_0(\cos\theta_s \cos 2\theta_i - \sin\theta_s \cos\phi_s \sin 2\theta_i)}\right] e^{-jk_o r} \tag{A.2.7}$$

For normal incidence ($\theta_i = 0$), $\bar{A}_{x_s}$ goes to zero and $\bar{A}_{z_s}$ reduces to equation (16).

It is clear from the presence of ϕ_s in expressions (A.2.6) and (A.2.7) that in general, for the case of oblique incidence, the fields are not symmetric about the axis of specular reflection. The field patterns can of course be computed from (A.2.6) and (A.2.7) for the general case. However at this point, it is interesting to examine the relativistic beam (large γ) case.

Based on the results for normal incidence, it is reasonable to expect that the radiation is concentrated in the $\theta_s = 1/\gamma$ region. Using small angle approximations for functions of θ_s and the usual relativistic relations between β and γ, (A.2.6) and (A.2.7) may be approximated by:

$$\bar{A}_{x_s}(r,\theta_s,\phi_s,\omega) \approx \frac{j\mu_0 \bar{I}_0(\omega)}{4\pi r k_0}(\tan\theta_i) e^{-jk_o r} \tag{A.2.8}$$

$$\bar{A}_{z_s}(r,\theta_s,\phi_s,\omega) \approx \frac{-j\mu_0 \bar{I}_0(\omega)}{4\pi r k_0}\left[\frac{2}{1/\gamma^2 + \theta_s^2} + \frac{1}{2}(1 - \tan^2\theta_i)\right] e^{-jk_o r} \tag{A.2.9}$$

For large γ, (A.2.8) and (A.2.9) are valid for all incident angles except for those approaching 90° (grazing incidence). The first term in the brackets of equation (A.2.9) is on the order of γ^2 for small θ_s. Clearly this term dominates the second term in the brackets and $\tan\theta_i$

in expression (A.2.8). Therefore, for large γ, the vector potential for the case of oblique incidence is well approximated by a single component in the direction of specular reflection:

$$\bar{A}_{z_s}(r,\theta_s,\omega) \approx \frac{-j\mu_0 \bar{I}_0(\omega)}{2\pi r k_0}\left(\frac{1}{1/\gamma^2+\theta_s^2}\right)e^{-jk_0 r} \qquad \text{(A.2.10)}$$

Expression (A.2.10) agrees with expression (16) in the main text for large γ. Therefore all of the field expressions for normal incidence are valid for oblique incidence for relativistic beams.